J. Fluid Mech. (1982), *vol.* 125, *pp.* 259–281
Printed in Great Britain

Convective pattern evolution and secondary instabilities

By J. P. GOLLUB, A. R. McCARRIAR AND J. F. STEINMAN
Physics Department, Haverford College, Haverford, PA 19041 and Physics Department, University of Pennsylvania, Philadelphia, PA 19104

(Received 26 February 1982 and in revised form 28 May 1982)

Using an automated laser-Doppler scanning technique, we have performed an extensive study of pattern evolution and instabilities in a large Rayleigh–Bénard cell (20 by 30 times the layer depth) at moderate Prandtl number (2·5). This work differs from earlier experiments in that the Doppler mapping technique permits both the spatial structure and time evolution of the velocity field to be quantitatively studied, and runs lasting up to ten thousand vertical thermal diffusion times are presented. We observe and document the properties of three qualitatively different regimes above the critical Rayeigh number R_c. (i) Below $5R_c$, there are a number of simple patterns in which the rolls align perpendicular to all lateral cell boundaries. The patterns are therefore curved and generally contain two boundary-related defects. A change in R induces patterns with many defects, which evolve toward the simple patterns over extraordinarily long times. These features seem to be consistent with theoretical models based on the competition between boundary, curvature and defect contributions to a Liapunov functional. However, stable states are not always reached. (ii) Above $5R_c$ the skewed-varicose instability of Busse & Clever causes progressively faster broadband time dependence with a spectral tail falling off approximately as the fourth power of the frequency. Doppler imaging shows that the fluctuations are caused by narrowing and pinching off of the rolls. (iii) Above $9R_c$ both the oscillatory and skewed-varicose instabilities cause local velocity fluctuations. However, substantial mean roll structure persists even over a 40 h period (one horizontal thermal diffusion time) at $15R_c$. Velocity power spectra with two distinct maxima associated with the two instabilities are still resolved at $50R_c$. Finally, we impose thermal inhomogeneities in order to pin the rolls, and show that the fluctuations are suppressed only if the local heat flux is a significant fraction of the convective heat transport per wavelength.

1. Introduction

Efforts to extend nonlinear stability theory and to understand the transition to turbulence have often focused on the problem of convective instabilities in a fluid layer of large horizontal extent (large aspect ratio). In the related small-aspect-ratio case, a variety of new phenomena have been recently discovered, including multiply periodic oscillations, phase locking, and sequences of subharmonic bifurcations. (For a review of the work of several different groups see Gollub (1982).) However, the dominance of boundary effects in small-aspect-ratio layers has precluded quantitative comparison of experimental results with theoretical computations, except in special cases.

On the other hand, there are well-defined theoretical predictions applicable to large-aspect-ratio layers. The Rayleigh–Bénard instability is expected to lead to a

time-independent steady flow of parallel rolls above the critical Rayleigh number R_c, and this remains true at least for two-dimensional flows when the effects of lateral boundaries are included (Cross *et al.* 1980, 1981). Subsequent instabilities depend on the Prandtl number, but in the region relevant to the present experiments (0·5–3), the spatially periodic 'skewed varicose' instability should first deform the rolls as R is increased (Busse & Clever 1979). The question of whether the resulting flow at finite amplitude is time-dependent or even noisy is unknown. At higher R the rolls are predicted to become unstable to a time-periodic deformation, the oscillatory instability, in which transverse waves propagate along the roll axis (Clever & Busse 1974). The existence of the skewed varicose and oscillatory instabilities has been confirmed experimentally, but the evolution of the resulting flows above their thresholds has not been studied with techniques capable of resolving the spatial structure quantitatively.

Important questions remain even at Rayleigh numbers below the onset of the secondary instabilities. How does the roll structure accommodate to the boundaries in large systems when variations of the velocity field in all three spatial dimensions are allowed? What are the mechanisms of pattern evolution? How do defects in the roll patterns affect their stability? Recent theoretical calculations based on an amplitude equation (see §4) have provided some theoretical progress in this area. However, experiments have been limited by the fact that pattern evolution can apparently last much longer than the horizontal thermal diffusion time, weeks or more in many earlier investigations. Furthermore, previously available probes measured either a horizontally averaged quantity (such as the heat flux) or a local quantity (such as the velocity). It has not been possible to perform simultaneous quantitative studies of both the spatial structure and its time evolution.

The experiments reported in this paper utilize a laser-Doppler mapping technique in which the spatial structure of the velocity field is mapped in a horizontal plane. Most importantly, the mapping can be accomplished in a time shorter than the characteristic times of velocity variations at low R, so that both the space and time structure of one component of the velocity field $\mathbf{v}(\mathbf{r}, t)$ are recorded in digital form, provided the time variations are sufficiently gradual. This technique was found to be a powerful tool for studying pattern evolution above R_c and the secondary instabilities that lead to progressively faster noisy time-dependence at higher R. Preliminary results were reported previously (Gollub & Steinman 1981).

The relationship of our work to other experiments and to theoretical studies can be more efficiently discussed in the context of the observations, so we proceed to a description of the experimental methods in §2 and results in §3. The reader interested in a concise summary is advised to read §5 (discussion and conclusions) first.

2. Experimental methods

2.1. *Convection cell and fluid*

The general design of the cell is shown in figure 1. The dimensions were selected to make the aspect ratio as large as possible consistent with the requirement of horizontal optical access through the thin edge. This permitted the horizontal surfaces to be thermally massive copper plates, which are separated by a Plexiglas spacer to produce a fluid volume of dimensions 15·24 cm by 10·16 cm by 0·522 cm high. The ratio of the largest horizontal dimension to the fluid depth is 29·2, and the ratio of the two horizontal dimensions is 1·5. (The anisotropy is important in determining the relative stability of different convection patterns near R_c.) The

temperature gradient at the lateral fluid boundary cannot be assumed to be accurately uniform, although good thermal contact between the copper and Plexiglas was maintained.

The experiments were conducted at about 70 °C, where the Prandtl number of water, the working fluid, is reduced to about 2·5, a value sufficiently low to permit comparison between our results and those obtained on liquid helium. The vertical and horizontal thermal diffusion times, the natural hydrodynamical timescales, are 170 s and 40 h respectively.

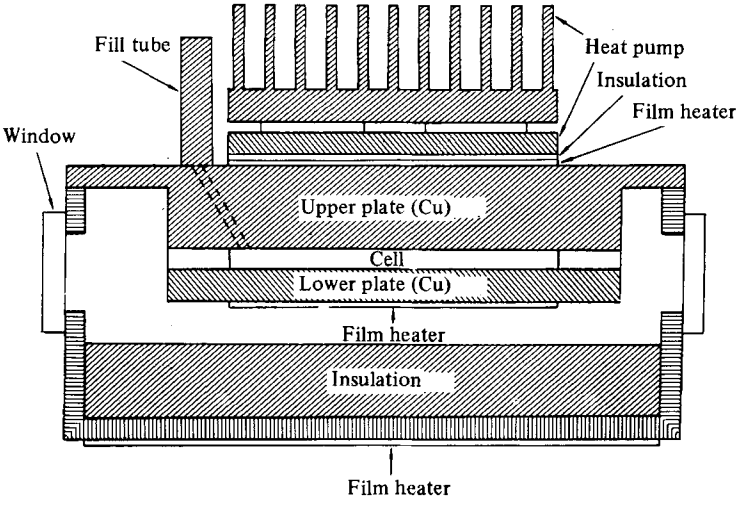

FIGURE 1. Schematic diagram of the convection cell showing the film heaters used to control the temperatures of the upper and lower copper plates and to maintain the outer heat shield at the mean working temperature; the thermoelectric heat pump used to provide a stable thermal reservoir for the heat transported through the fluid; and the windows for laser-Doppler access.

The fluid is rather close to the Boussinesq approximation under the conditions of the experiment. The variation of the Prandtl number from its value at the midplane of the cell was at most 4 % even at $50R_c$, the highest Rayleigh number studied. For Rayleigh numbers below $10R_c$, where we seek quantitative comparison with the predictions of stability theory, the Boussinesq approximation may be considered to apply accurately.

In order to prevent excessive radiative heat transfer from the cell, it is surrounded by a copper heat shield controlled at the mean working temperature (± 1 K). The horizontal copper plates are maintained at constant temperature by two electronic feedback systems based on a.c. bridges and lock-in amplifiers. The d.c. output of each lock-in drives a resistive film heater via an operational power supply. Three thermistors are embedded in each plate, one for the control loop, and two for monitoring the temperature and its horizontal gradient, if any. Styrofoam insulation surrounds the cell except in the area of the windows. Whereas our previous work (Gollub & Benson 1980) utilized vacuum isolation, we found that the present arrangement provided comparable performance. In order to reduce further the sensitivity of the system to ambient temperature variations, and to provide a more effective means of dissipating the large heat flux at high R (about 50 W at $50R_c$), we installed a copper cold plate separated from the upper plate of the convection cell by a thin insulator, and controlled its temperature with a thermoelectric heat pump

and an aluminium heat sink. Thus the environment seen by the convection cell is the cold plate of the thermoelectric heat pump rather than the room air. This plate was maintained constant to within about 0·1 K by a d.c. control loop.

This combination of four temperature control systems (upper and lower plate, thermoelectric heat pump, and heat shield) was required in order to achieve a temperature stability of approximately ± 2 mK at low R over periods of several weeks, the duration of a typical experiment. This corresponds to a stability of better than 1 % in R at $2R_c$. At higher R, the spatially inhomogeneous and time-varying effective thermal conductivity of the fluid degrades the temperature stability somewhat, to ± 10 mK at $20R_c$, but the fluctuations expressed as a fraction of R/R_c are then less than 0·5 %. The horizontal variation in R over the full width of the cell is measured to be about 3 % at $2R_c$.

During some of the experiments a Teflon-coated constantan wire was inserted in the cell parallel to and 3 cm from one of the short edges, and 0·6 mm above the lower plate. This wire was used as a local heat source to determine the response of the system to horizontal thermal inhomogeneities.

2.2. *Doppler imaging*

Laser-Doppler velocimetry was the primary measurement tool in this study. As in our previous work at small aspect ratio (Gollub & Benson 1980) we use a real-fringe forward-scattering technique with two horizontally propagating beams intersecting at a point in the cell. The beams have a relative offset of 2000 Hz in order to eliminate directional ambiguity in the velocity measurement. The optics are similar to those described previously, except for minor changes necessitated by the increased size of the convection cell. The beam-intersection angle is 6·8° in the fluid, resulting in an ellipsoidal scattering volume whose longitudinal and transverse dimensions are about 2 mm and 0·1 mm respectively.

The optical system is sensitive to the horizontal velocity component transverse (perpendicular) to the bisector of the beams. This is also the component parallel to the longest dimension of the cell. The conversion between frequency shift and velocity is $4{\cdot}0 \times 10^{-4}$ cm s^{-1} Hz^{-1}.

The flow system is mounted on computer-controlled translation stages to permit the velocity to be mapped in a horizontal plane. As a precaution, the velocity of the stage is ramped when starting and stopping to reduce the acceleration. We have not found evidence of any effect on the fluid of moving it in the mapping process. The minimum time required to translate the cell 1 mm and read the velocity with signal-to-noise ratio of about 30 is 1·5 s. While this is a fairly long time, the velocity fluctuations are often so slow that a region of the cell including a few rolls can be imaged (by a few hundred point measurements) before significant changes occur. Below about $5R_c$, where the time-dependence is either absent or very slow indeed, the entire cell can be accurately mapped (a few thousand point measurements). In addition to the Doppler imaging of the roll structure, we made local velocity measurements over long time periods and computed power spectra using the methods described by Gollub & Benson (1980).

3. Experimental results

3.1. *Simple convective patterns*

We invested considerable effort in the determination of the nature, variety, and stability of convective flow patterns above R_c in our system, because most previous large-aspect-ratio experiments did not extend to times comparable to the horizontal

thermal diffusion time (40 h in our system, weeks in some previous experiments). We found that runs at least this long are required in order to determine the form and stability of convective flows.

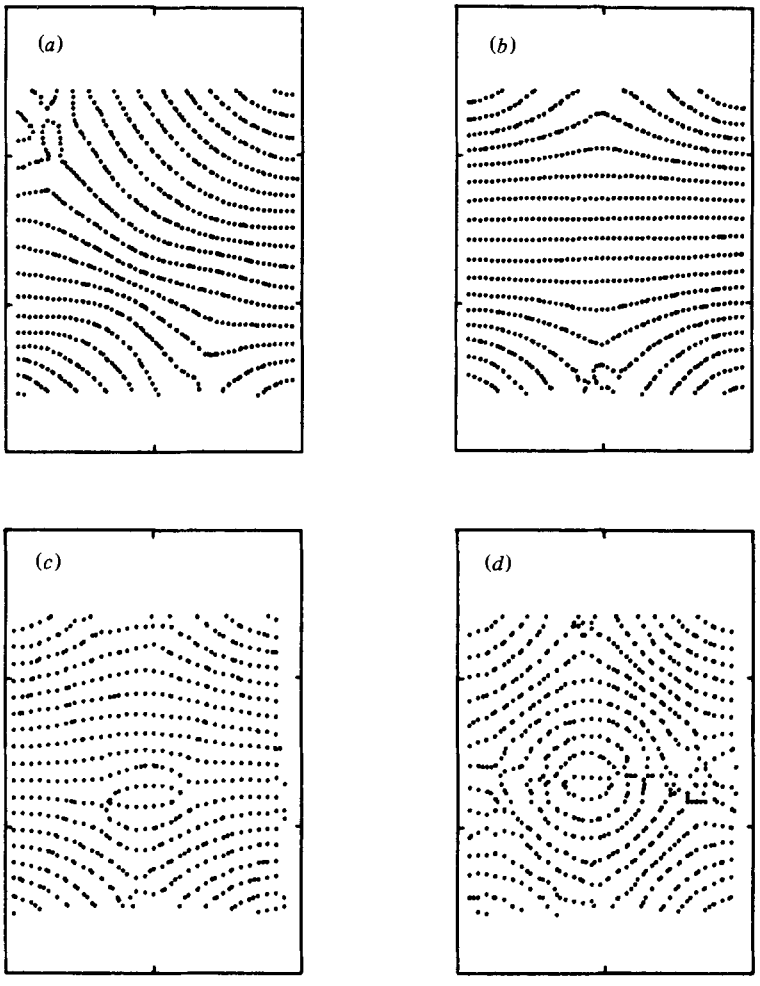

FIGURE 2. (*a*, *b*) Contour maps showing stable patterns at $4R_c$ long after R was reduced from above $5R_c$. Each dot is a point at which the velocity component parallel to the long cell edge is zero. The loci of these points mark the roll boundaries, in a horizontal plane above the centre of the cell. The rolls are always perpendicular to the lateral boundaries. (The blank regions are outside the field of view of the optical system.) (*c*) Stable pattern with a bound defect pair at $2R_c$ after slowly exceeding the threshold. (*d*) Transient pattern at $2R_c$ with circular region in the centre after rapidly exceeding the threshold.

Experiments were performed with different initial conditions, and a variety of patterns were obtained after one or two horizontal thermal diffusion times. Figures 2(*a*–*c*) show some of the simplest patterns found to be stable over many days. These contour maps are composed of dots at all locations where the velocity component parallel to the long cell edge is found to be zero. The dot spacing is a measure of the density of points in the grid pattern of velocity measurements. For each map the velocity was measured at 2646 points. The locus of these dots represents the boundaries of the convective rolls, in a horizontal plane above the centre of the cell. (However, the patterns must be cautiously interpreted where the rolls are locally

parallel to the long cell edge, because the probe is then insensitive to the dominant velocity component, and spurious zero crossings can then occur.)

The salient feature of figure 2 is the fact that the rolls align approximately perpendicular to all of the lateral cell boundaries. (We assume that there are no surprises in the strips lying outside the field of view.) Perpendicular alignment is found in all the maps we have made below $5R_c$. One important consequence is that the roll pattern is splayed and contains defects, where a roll (or sometimes a pair of rolls) ends. Two defects is apparently the minimum number consistent with perpendicular boundary alignment and is the minimum number we have observed in many experiments. Figure 2(*c*) shows an extra pair of defects in the centre of the cell, which seems to be stable indefinitely (at $2R_c$).

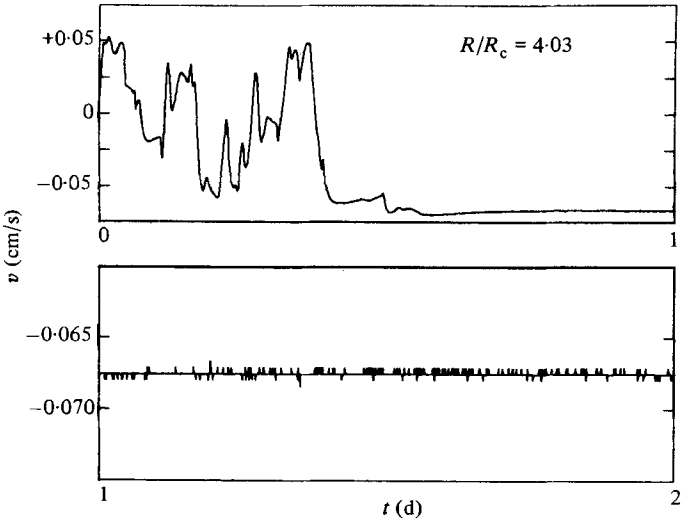

FIGURE 3. Transient time dependence of the velocity at the midpoint of the cell after R was reduced fron $5{\cdot}6R_c$ to $4{\cdot}0R_c$. The lower section (second day of the run), shown on an expanded scale, is time-independent to within the experimental resolution, about 1 Hz Doppler shift (height of the marks).

We find that both symmetric and asymmetric patterns are observed under the same external conditions. Furthermore, the asymmetric pattern of figure 2(*a*) is found on other occasions approximately reflected about the long axis of the cell. These observations indicate that the asymmetries do not result from small horizontal temperature gradients. Rather, they represent different solutions to the hydrodynamic equations resulting from different initial conditions.

Are these patterns strictly time-independent? In figure 3 we show the transient (measured at a single point) that led to the pattern of figure 2(*a*). The velocity component parallel to the long cell edge is plotted as a function of time at the centre of the cell (but above the midplane) after R was reduced from $5{\cdot}6R_c$ to $4{\cdot}0R_c$. The flow was time-dependent before the change, and the time dependence continues for nearly a day before dying out. During the second day of the record, shown on an expanded scale, the fluctuations (if any) are less than the instrumental noise level of 1 Hz in the Doppler shift, or 1% of the maximum velocity in the flow. (This is the height of the tick marks on the graph.) In order to test further the time-independence of the flow, we made a second map one day later, and found that it could be superimposed on that of figure 2(*a*) to within a few per cent of the roll

spacing. The stability of the flows shown in figures 2(*b*, *c*) is comparable. Of course the possibility of further change on a very long timescale cannot be excluded. (In §3.2 we note that stable flows are not always observed even after long times.)

The simple patterns of figures 2(*a*, *b*) can often (but not always) be created by holding R just above $5R_c$ for a day or so, and then decreasing it to a value somewhat below $5R_c$. (We show in §3.4 that there is intrinsic time dependence resulting from the skewed varicose instability above $5R_c$.) However, it is in general not possible to reproduce the initial conditions precisely enough to select a desired pattern upon demand. Of course, this could presumably be done approximately by imposing an initial thermal perturbation of the desired form (Chen & Whitehead 1968).

The roughly circular pattern of figure 2(*d*) is a special case. It was obtained after R was suddenly increased to $2R_c$ from $0{\cdot}5R_c$. The fact that the pattern is roughly circular in the central region (except for the smallest ring, which is divided) seems remarkable. This pattern is less stable than the others in figure 2; the circular symmetry lasts approximately one day.

3.2. *Pattern evolution*

In this section we present several examples of pattern evolution over very long times, in the regime between R_c and $5R_c$ where parallel rolls are predicted to be stable. Figure 4 shows a sequence of contour maps over a 229 h period following an increase in R from $0{\cdot}4R_c$ to $2{\cdot}05R_c$. Times are given both in hours and parenthetically in units of the vertical thermal diffusion time. The first map was started just after R was established at its new value, and each map required several hours to complete. Since the time dependence is initially significant on this timescale, the first few maps are not quantitatively accurate.

It is evident that the pattern is complex at first, presumably owing to the nucleation of convective domains of differing roll orientation. (When R_c is exceeded slowly instead of quickly, this complexity at early times is missing.) Eventually the pattern becomes much simpler, but the simplification is not gradual in this run. Rather, there is an obvious change between 12 and 15 h (260 and 320 vertical thermal diffusion times) after the start of the run. The pattern continues to evolve, and reaches an apparently stable state at 96 h. There is negligible change between 96 and 229 h. This pattern, though not as simple as those of figure 2, is stable for a surprisingly long time (perhaps indefinitely).

The map at 64 h in figure 4 shows a clear example of a defect where two rolls are annihilated in the centre of the cell. We find that defects not associated with large-scale curvature in the roll pattern are generally unstable and disappear by translating across the pattern. A defect may involve the termination of either one roll or two adjacent rolls (and there may be other possibilities as well). We have not made a systematic study of isolated defects because they are transitory. However, they could be produced at will by suitable initial conditions. We observe that the nucleation and motion of defects are an important mechanism of pattern evolution, but they do not seem to be the only cause of that evolution.

Another example of slow pattern evolution is shown in figure 5. In this case, R had been raised slowly to $1{\cdot}55R_c$ and left for 350 h, but the flow was still clearly time-dependent. The Rayleigh number was then increased to $3{\cdot}66R_c$ in order to determine whether stabilization would then occur, and about 100 maps were made over the next 400 h. The increase in R causes a region of many defects to appear in the cell after 28 h. The pattern changes somewhat, but preserves its overall structure at least until 129 h, an interval of more than 2000 vertical thermal diffusion times

(2·5 horizontal thermal diffusion times). At 162 h a major change in the overall structure is obvious, and evolution continues, at a decreasing rate, up to the end of the run. The last two maps are similar to each other, but many of the contours show a relative shift of about half of the roll spacing. Our experience suggests that the overall pattern will remain qualitatively the same, but continued gradual evolution cannot be excluded.

These examples demonstrate that pattern evolution can produce many different flow histories for different initial conditions. We also tested the repeatability of the evolution process following a sudden increase in R from $0{\cdot}5R_c$ to $2R_c$. In each of ten experiments a pattern with many defects is produced initially which evolves on a

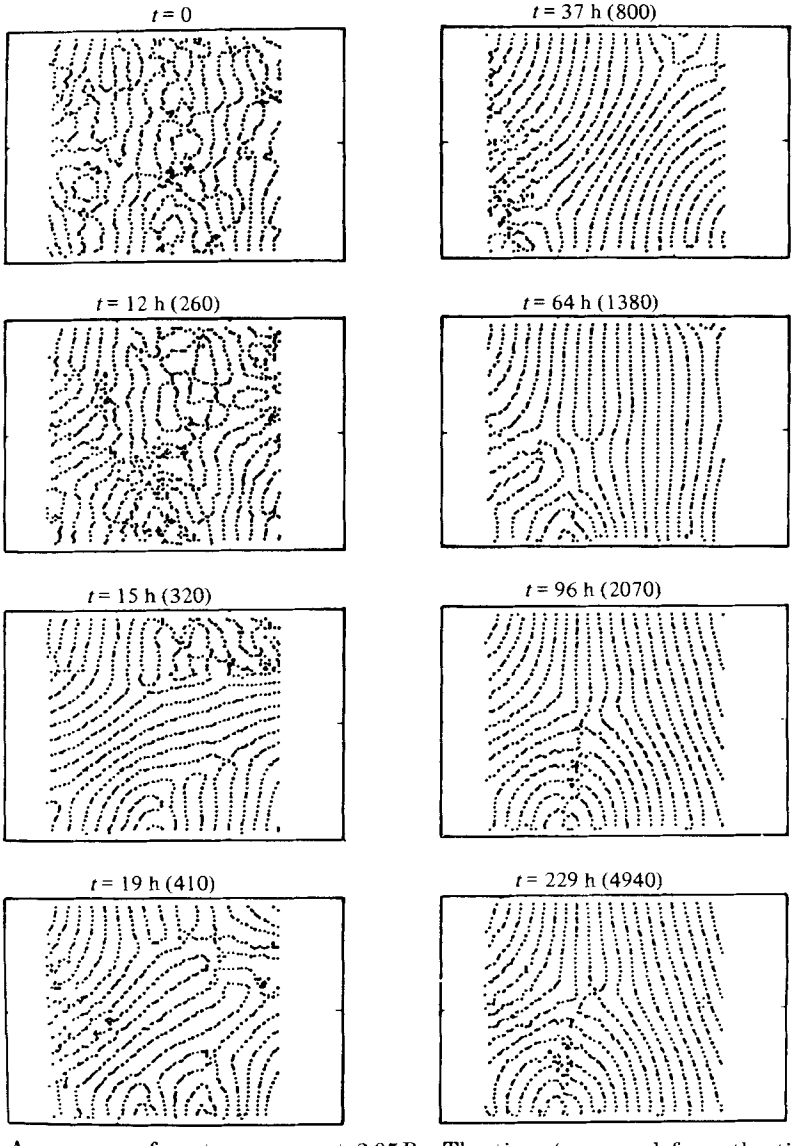

FIGURE 4. A sequence of contour maps at $2{\cdot}05R_c$. The time (measured from the time R_c was exceeded) is shown in both real time (hours) and non-dimensional time (units of the vertical thermal diffusion time). The pattern is complex at first and eventually stabilizes in a simpler (but still asymmetric) form.

timescale shorter than a few hundred vertical thermal diffusion times. However, the patterns are different in each experiment. After a few thousand vertical diffusion times a simpler pattern with only boundary-related defects is always present. These simpler patterns (not limited to those of figure 2) tend to be stable or nearly stable over much longer times. However, a strictly stable state is not always reached even in a few hundred hours, a time much greater than the horizontal diffusion time.

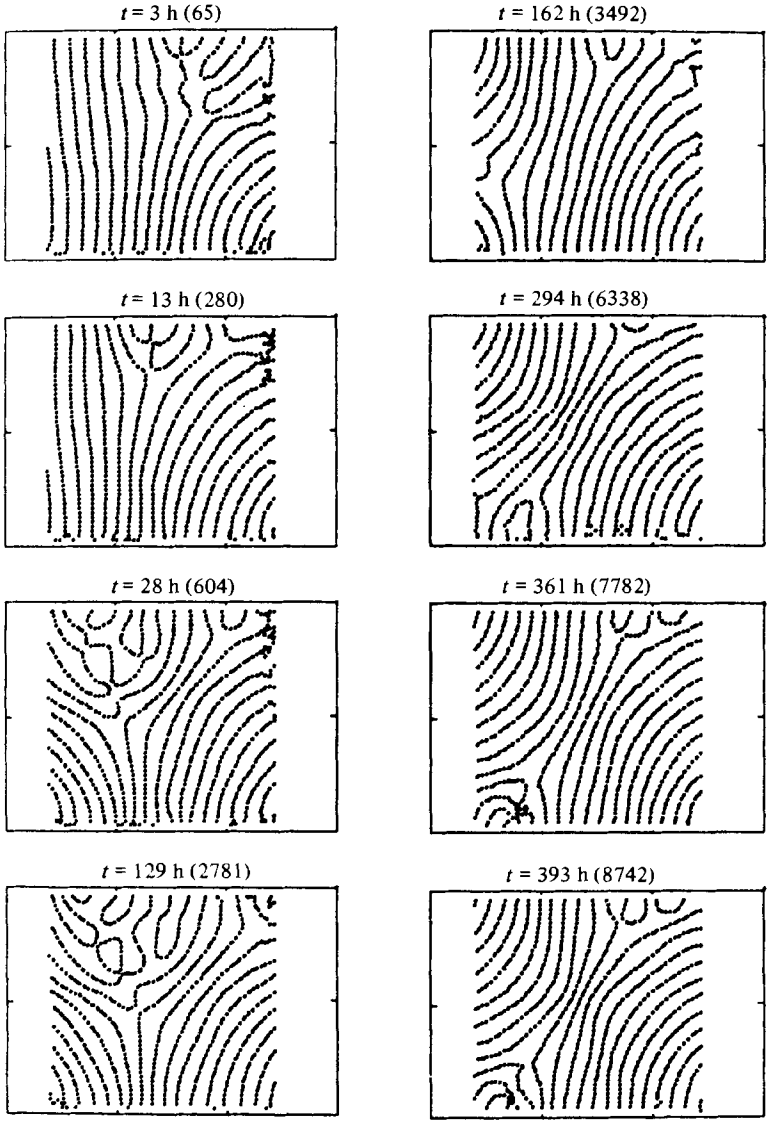

FIGURE 5. A sequence of contour maps at $3{\cdot}66R_c$ after R was raised from $1{\cdot}55R_c$. A very complex pattern with many defects persists for about 100 h (from 28 to 129 h) and then changes dramatically to a much simpler pattern.

3.3. *Overview of time-dependence above* $5R_c$

The slow pattern evolution discussed in §3.2 is quite different from the much faster time dependence that always occurs above a transition point R_1 located at $(5{\cdot}0 \pm 0{\cdot}5)R_c$, with only slight dependence on initial conditions.

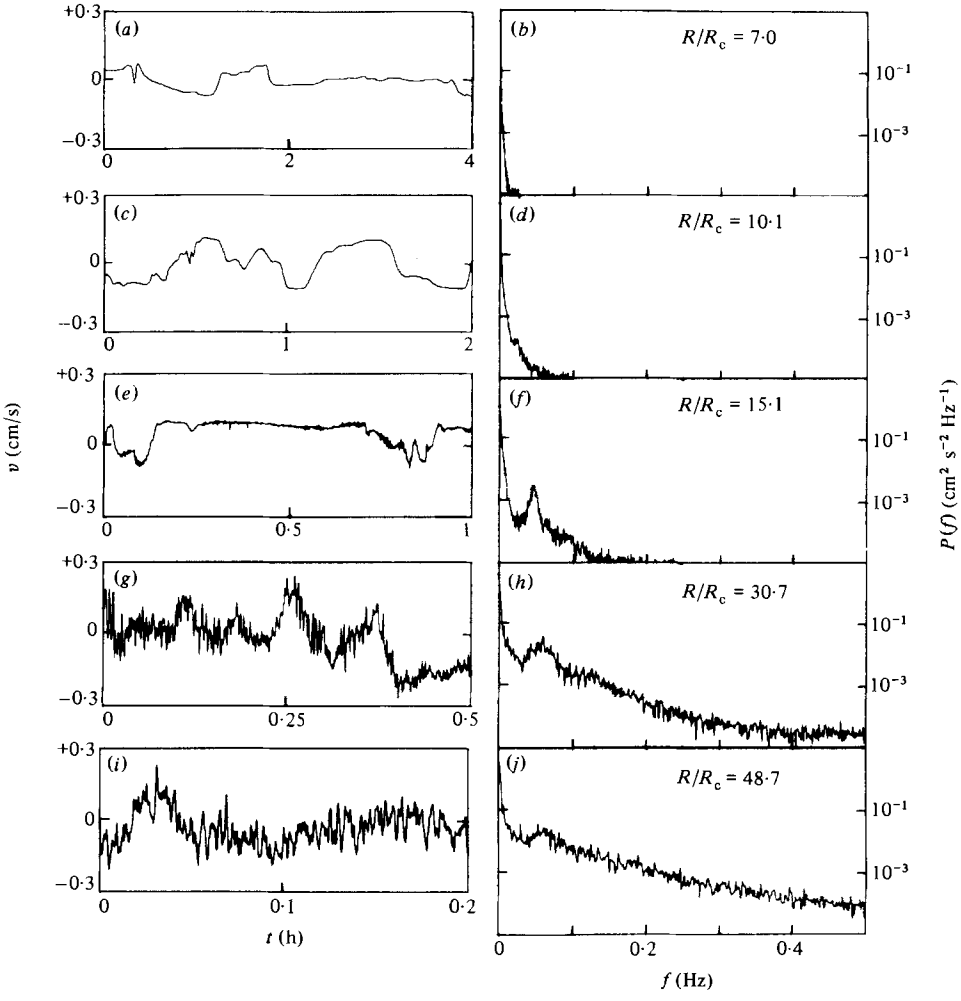

FIGURE 6. Overview of time-dependent phenomena. Velocity records and corresponding spectra are shown at five values of the Rayleigh number. The dominant spectral features are the peak at zero frequency with onset near $R_1 = 5R_c$ and the peak at about 0·05 Hz with onset near $R_2 = 9R_c$. These features are identified with the skewed varicose and oscillatory instabilities, respectively (see §5).

An overview of the time-dependent regimes above R_1 is shown in figure 6. The velocity as a function of time at a point near (but above) the centre of the cell is shown for six different Rayleigh numbers chosen to illustrate the range of observed phenomena. Each time record is accompanied by a power spectrum, shown on a logarithmic vertical scale. While the timescale changes by a factor of two from one time record to the next, the power spectra are all on the same frequency scale. At $7R_c$, somewhat above R_1, the velocity fluctuates slowly with a mean value close to zero. The corresponding spectrum (figure 6*b*) has a maximum at zero frequency, and

decreases smoothly into the instrumental background, located approximately at the bottom of the figure. We return later to a discussion of the detailed shape of this spectrum.

At a second transition $R_2 = (9 \pm 1)R_c$, oscillations with a frequency of about 0·05 Hz appear in the velocity record, though they are too small and too intermittent to be visible in figure 6(*c*). Their presence is manifested by a small shoulder in the power spectrum at $10R_c$ (figure 6*d*). At $15{\cdot}1R_c$, this peak is quite prominent, and at $30{\cdot}1R_c$ it has begun to merge with the peak centred at zero frequency. However, these two dominant spectral features are both still visible at $48{\cdot}7R_c$ (figure 6*j*).

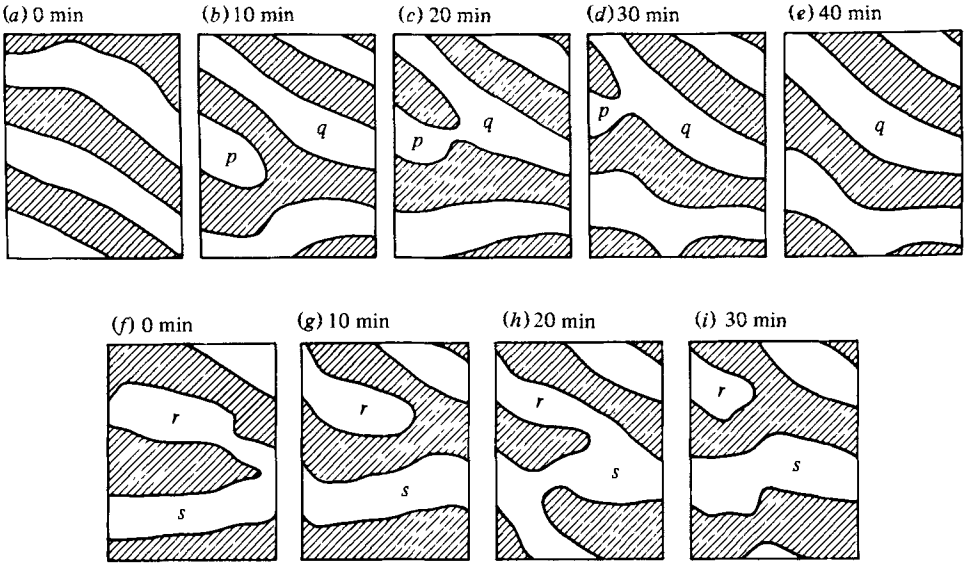

FIGURE 7. Two sequences of Doppler images showing a portion of the velocity field at intervals of 10 min, at $R = 5R_c$. Shaded and unshaded regions have opposite vorticity. The rolls are clearly unstable, and repetitively undergo a narrowing and pinching-off process (see §3.1) that is probably caused by the skewed varicose instability.

3.4. *Instability at R_1: spatial behaviour*

In this section we present maps of the intrinsic time dependence that appears at $R_1 \approx 5R_c$. It is clear that spatial information is required to identify the cause of the fluctuations. Fortunately, the timescale is so slow that we are able to image a region of the cell containing a few rolls before the pattern changes substantially.

Figure 7 shows sequences of maps made at 10 min intervals at $5R_c$, just above R_1. Each map is constructed from 160 velocity measurements covering a 4×5 cm region of the cell. The lines connect points at which the interpolated Doppler shift is zero, i.e. the roll boundaries. Rolls circulating in one sense are shaded. While these images are not strictly instantaneous, they are nearly so. (Furthermore, the raster pattern consists of a sequence of lines parallel to the long axis of the cell. Since nearby lines are measured close together in time, the patterns are locally accurate even if the overall pattern does change somewhat during the 10 min interval required to generate the map.)

In figure 7(*b*) the intrusion of a defect *p* is visible. In figure 7(*c*) it merges with a roll *q* of similar vorticity, and a new defect (now shaded) is expelled from the field of view. A second sequence begins in figure 7(*f*), where a roll labelled *r* is pinched

off to form a defect, merges with region s (figure 7h), and is then separated again (figure 7i).

Hundreds of such maps have been made. The structural changes shown in figure 7 are typical of the fluctuations just above R_1. We interpret this persistent structural motion as an indication that the rolls are unstable in this regime. However, the activity is somewhat intermittent. In some cases, the imaged portion of the cell is relatively quiescent for tens of vertical thermal diffusion times.

The mean roll wavenumber is known to decrease with wavenumber. We find that much of this decline occurs in the neighbourhood of the instability at R_1. Some evidence for the wavenumber decline is presented in §§3.6 and 3.7 (figures 12 and 14). In addition, we have made two-dimensional Fourier transforms of the digitized velocity field, in order to study wavenumber variations quantitatively. This work is reported in a separate paper (Gollub & McCarriar 1982), and a substantial decrease in the mean roll wavenumber near R_1 is clearly found by this technique as well.

3.5. *Instability at R_1: statistics*

Statistical information obtained from the time dependence at isolated points is also useful in characterizing and identifying the cause of the structural instability. The variation with R of the square root of the second moment of the spectrum, scaled by the inverse of the vertical diffusion time to obtain a dimensionless characteristic frequency, is shown in figure 8. (The moment calculation is cut off above 0·025 Hz to eliminate contributions from the peak due to the oscillatory instability above R_2.) The crosses are intended to indicate that there is no time dependence below R_1 (setting aside the exceedingly slow residual pattern evolution sometimes observed). Note that the characteristic frequency increases approximately linearly with R above R_1, though it seems to be finite at R_1. The inverse of the characteristic frequency is rather long (about 3000 s at $5R_c$, a fact that is crucial for Doppler imaging.

We have also examined the question of whether there is hysteresis in the transition at R_1. We find some variability in the position of R_1 ($\pm 0{\cdot}5R_c$), but this seems to be associated with variations in the spatial structure from run to run rather than with genuine hysteresis in the position of R_1 for a single pattern. We could not trace out a hysteresis loop.

The shapes of the power spectra above R_1 have been studied in some detail. An example is shown in figure 9, along with the accompanying time record. A log–log scale is used for the spectrum in order to exhibit the high-frequency behaviour more clearly. The spectrum is flat at low frequencies, and falls off approximately as a power law at 'high' frequencies. However, there is not a long region that is demonstrably a power law. There is perhaps some slight curvature in the spectrum, suggesting that a power-law fit is at best a crude approximation. The spectrum cannot be extended to higher frequencies (and small amplitudes) because of the experimental noise level, which is about 10^{-6} cm^2 s^{-2} Hz^{-1}, six orders of magnitude below the maximum power.

Although power-law fits are not very accurate, we present in figure 10 the best-fitting exponent as a function of R. The exponent is generally between -4 and -5. The error bars represent the statistical errors only. However, the exponent also depends slightly on the cutoff used to define the high-frequency region of the spectrum. This fact, together with the observation that the variability of n is somewhat larger than the error bars, indicates that the notion of a power-law tail is probably at best approximate.

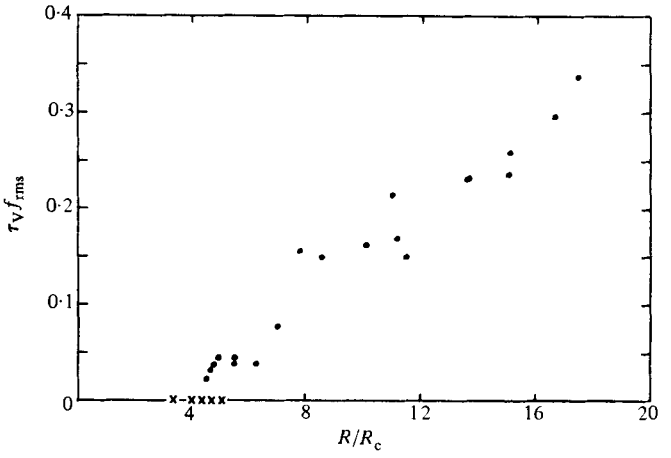

FIGURE 8. The square root of the second moment of the velocity power spectra (below 0·025 Hz), scaled by the inverse vertical thermal diffusion time, as a function of Rayleigh number. Crosses indicate that there is no time dependence below a threshold near $5R_c$, except for exceedingly slow residual pattern evolution in some cases.

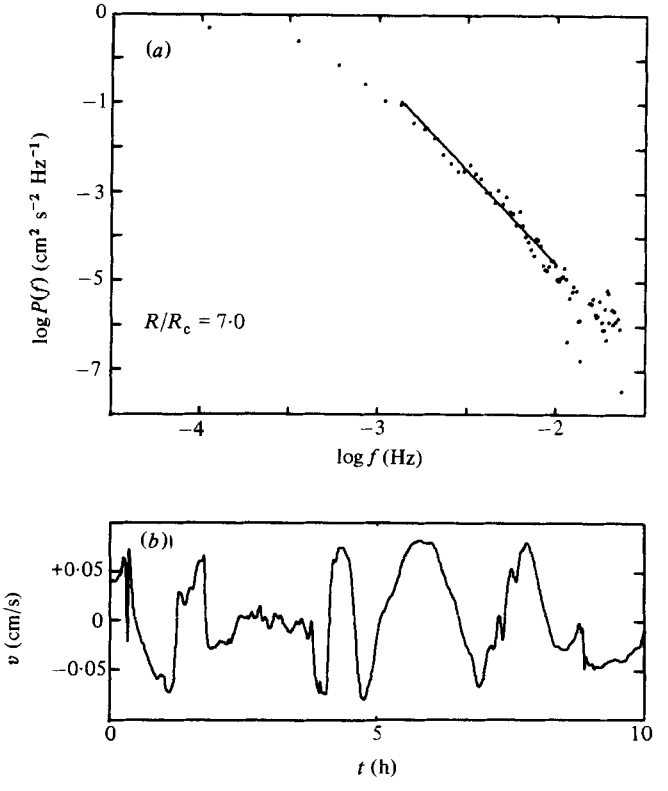

FIGURE 9. A typical velocity power spectrum above R_1, plotted on log–log scales to exhibit the shape of the tail more clearly, and the corresponding time record. While a power law (straight line) can be fitted to the spectrum at high frequencies, there appears to be some residual curvature.

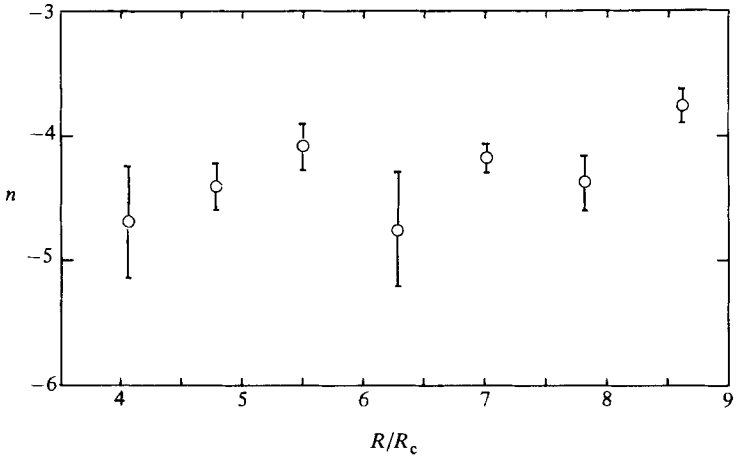

FIGURE 10. Exponent n of power-law fits to the spectra, as a function of Rayleigh number. The variation is somewhat larger than the statistical error bars, but the exponent is usually between -4 and -5.

3.6. *Instability at* R_2

Above a threshold at $R_2 = (9 \pm 1) R_c$, a broad peak at finite frequency is clearly visible in the power spectrum of the local velocity, as shown in figure 6. In order to study this instability quantitatively, we computed the area under the spectral peak, and the results are presented as a function of R in figure 11 (a). There is significant variability in the peak area from run to run, because of the intermittency of the oscillations. We believe that the temporal intermittency is a consequence of spatial intermittency, as previous visual observations have indicated. The data indicate that the amplitude of the oscillations grows smoothly from zero as R is increased above R_2. The mean frequency f^* of the peak also increases smoothly with R above the onset at R_2, as shown in figure 11 (b).

At $15R_c$, the instabilities at R_1 and R_2 produce large-amplitude random time dependence. Therefore one might expect the roll structure to vanish in the mean. To test this hypothesis, we generated 50 contour maps over a 40 h run, and averaged them at each point. Each map contained 875 points covering a $10 \times 10{\cdot}5$ cm region of the cell. The time (50 min) required to generate each map was much longer than the inverse of the root-mean-square frequency at $15R_c$, so the sampled velocities at corresponding points in the map should be statistically independent of each other. Several examples of 40 h mean contour maps, made one month apart, are shown in figure 12. Well-defined roll structures are still visible in these maps; the strength is about 25% of the instantaneous roll amplitude. However, the patterns are quite different in the two cases shown. The structure might average to zero over a much longer time. Nevertheless, it seems remarkable that strong correlations persist over a thousand vertical thermal diffusion times. At higher Rayleigh numbers ($40R_c$) we do find that a 40 h average is sufficiently long to wash out the pattern.

Another noteworthy feature of figure 12 is the large wavelength of the rolls. Both individual and mean maps show rolls with wavelengths about twice the critical value near onset (see e.g. figure 4). A large part of this change is found to occur at the transition R_1.

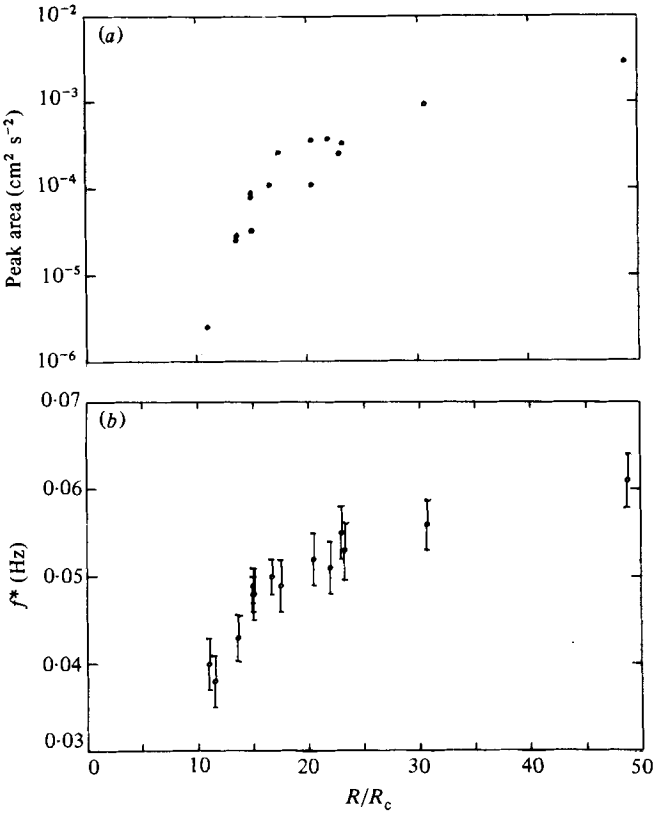

FIGURE 11. Properties of the spectral peak due to the oscillatory instability as a function of Rayleigh number. (*a*) Integrated area, which increases smoothly above an onset at $R_2 = 9R_c$ (see figure 6). (*b*) First moment f^*.

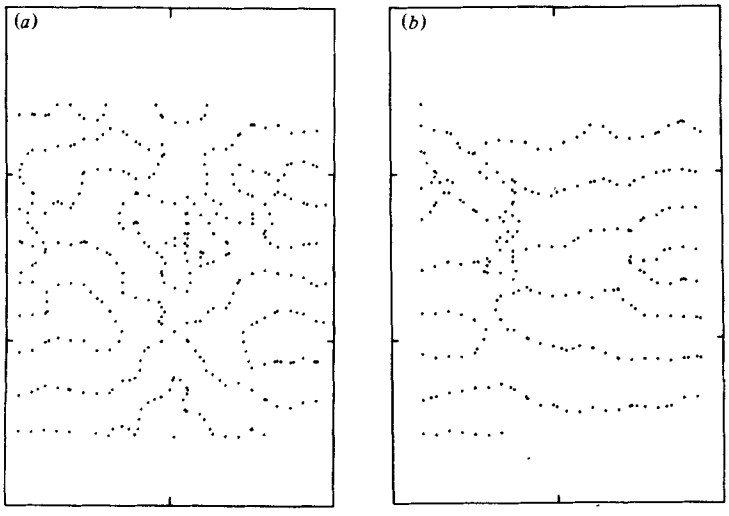

FIGURE 12. Mean contour maps over 40 h periods, on two different occasions, at $15R_c$. Although the motion is chaotic, considerable mean structure persists on this timescale. The solid line is the cell boundary (10 × 15 cm); the increase in wavelength above the critical value is obvious by comparison with figure 4.

3.7. *Roll-pinning experiments*

In order to obtain a quantitative measure of the strength of the fluctuations, we generated a horizontal anisotropy by means of a line source of heat parallel to the short side of the cell. This was accomplished using a Teflon-coated current-carrying wire (§2.1). In the time-independent regime, a heat input h, small compared with the total heat flow, is sufficient to align the rolls with the wire over more than half of the cell. In figure 13 for example, $h = 0{\cdot}09$ W, while the total flux through the cell is a factor of 30 larger. Since we made no attempt to determine the minimum value of h needed to pin the rolls, it is possible that substantially less would still be sufficient.

FIGURE 13. Pinning of the rolls by a line source of heat (located at the position of the solid line) in the time-independent regime.

In the time-dependent regimes, the rolls are pinned most strongly near the wire. The time-averaged velocity as a function of the distance from the wire is shown in figure 14 at $30{\cdot}5R_c$. The velocity averages to zero far from the wire, but the mean velocity near the wire is not appreciably weaker than the instantaneous velocity there. The long roll wavelength at high R can also be easily seen in figure 14.

The effect of local heating on the time-dependence is shown in figure 15. Velocity records and spectra taken close to (3 mm from) the wire are shown for zero and non-zero heat input. The local heating almost completely suppresses the velocity fluctuations near the wire. Corresponding spectra show suppression at all frequencies, with a particularly strong effect at low frequencies. (The suppression is stronger than it appears owing to the logarithmic scale.) We use the total low-frequency spectral power (below 0·025 Hz) as a measure of the strength of the fluctuations, and plot the logarithm of this quantity as a function of heater power h (for two different values of R) in figure 16. At $15R_c$, the trend is approximately linear on the semilog scale, implying that the low-frequency spectral power may be approximately represented by the equation $P = P_0 \exp(-h/H_0)$, where the attentuation constant H_0 is

approximately 0·27 W at $15R_c$. For comparison, H_0 is 14 % of the heat flux carried per wavelength (two rolls). We find that H_0 does not vary substantially with R above about $10R_c$. We have not been able to make a detailed investigation at lower R because the slow timescale of the fluctuations makes the data aquisition prohibitively time-consuming.

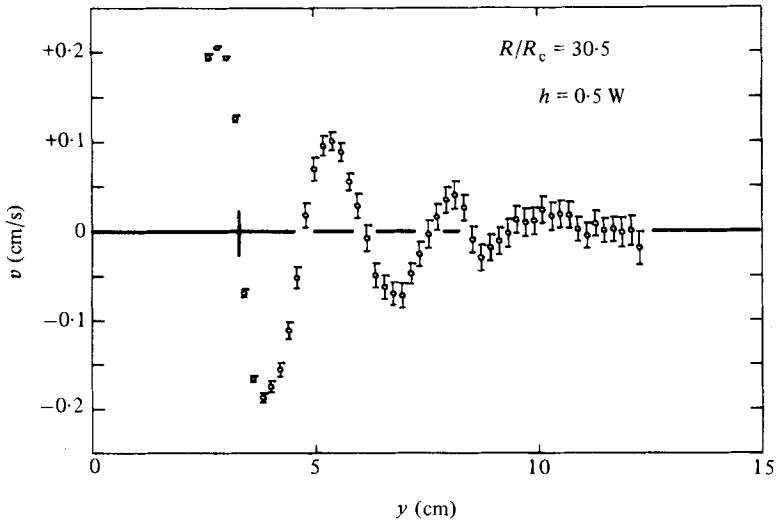

FIGURE 14. Pinning of the rolls by a line source of heat at high R. The mean velocity is shown as a function of distance from the source, which is located at the short vertical line. Note the long roll wavelength.

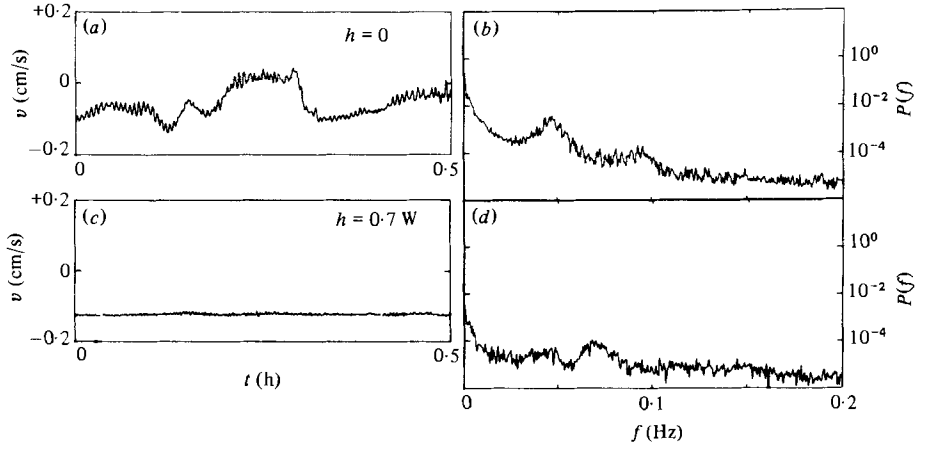

FIGURE 15. Effect of a line source of heat on the fluctuations. (*a*, *b*) Velocity records near the wire without heat input ($h = 0$) and with heat applied ($h = 0{\cdot}7$ W). (*c*, *d*) Corresponding spectra showing almost complete suppression of the fluctuations by the local heat source. The dashed line is the instrumental noise level, and the logarithmic scale should be noted.

We conclude from these experiments that the fluctuations resulting from the instabilities at R_1 and R_2 are robust, since the local heat flux required to suppress them is a significant fraction of the convective heat flux carred per wavelength.

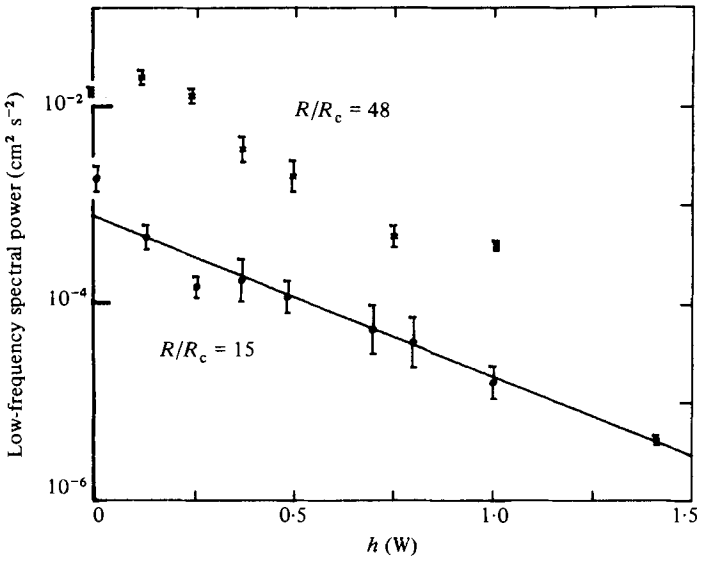

FIGURE 16. Low-frequency spectral power as a function of local heat input at two different Rayleigh numbers. The suppression of the fluctuations is approximately exponential.

4. Related theory and experiments

Some features of the results described in §3 have been noted previously. In this section we discuss the relationship of our results to other experiments, stability theories, and numerical computations.

4.1. *Stable flows in finite geometries*

The existence of several different stable convective flow patterns under the same external conditions has been nicely documented by Kirchartz *et al.* (1981) for the case of a cylindrical cell of diameter-to-height ratio 6. They used a novel technique based on differential optical interferometry to determine three-dimensional density profiles, and showed that either axisymmetric or non-axisymmetric flows can be obtained, depending on the rate of change of R. Because our rectangular cell is much larger and does not have rotational symmetry, it seems reasonable to expect a much greater variety of flow patterns than they found.

The alignment of rolls perpendicular to the long edges in rectangular cells was predicted by Davis (1967) and Segel (1969), was noted by Krishnamurti (1973) and Stork & Müller (1972), and is also apparent in photographs presented recently by Bergé (1981). We find that in a sufficiently large cell the alignment is perpendicular to all cell edges, not just the long ones. This fact seems not to have been predicted earlier because of the mathematical difficulty of handling curved rolls. It may not have been clearly documented in the experimental literature in part because of the exceedingly long transients in large cells.

The problem of finding the stable states in a finite container was considered theoretically by Cross *et al.* (1980, 1983) for two-dimensional motion slightly above threshold. They generalized the amplitude equations of Newell & Whitehead (1969) and Segel (1969) to show that the presence of sidewalls, no matter how distant, restricts the allowed wavevectors of stationary states. Cross (1982) has discussed the use of a Lyapunov functional F, whose minimization governs the relative stability

of various possible patterns not far above threshold. He showed that two competing contributions to F could be identified: a boundary contribution favouring roll orientation normal to lateral boundaries, and bulk contribution opposing rapid spatial variations in the local roll orientation. Defects were also shown to increase F, and are therefore unfavourable. The competition between these contributions to F is predicted to determine the relative stability of different patterns near onset. However, at higher R, especially near the onset of the skewed varicose instability, a potential theory is not expected to apply (Siggia & Zippelius 1981*a*).

4.2. *Evolution of patterns*

The gradual evolution of convective patterns not far above R_c is well known (see e.g. Krishnamurti 1970). Often this has been considered a nuisance to be overcome by imposing an initial spatially periodic perturbation and studying the stability of the resulting flow before the pattern evolution has become significant (Chen & Whitehead 1968). Our perspective is somewhat different, since we seek to understand the evolution process in finite geometries. The fact that defect motion plays a role in pattern evolution has been noted by Whitehead (1976).

Ahlers & Behringer (1978, 1979) have reported sensitive heat-flux measurements on convecting liquid helium that may be relevant to the problem of pattern evolution. They found time dependence to be present immediately above R_c in a very large cell whose radius-to-depth ratio is 57. Subsequently, Ahlers & Walden (1980) found that time dependence in the form of a very slow background variation and randomly spaced larger events is present not far above R_c even for a smaller cell of radius-to-depth ratio 4·72, and observations of time dependence fairly close to R_c were also made by Behringer *et al.* (1981). The experiments of Ahlers & Walden were discussed by Greenside *et al.* (1982) in terms of a stochastic model of a particle diffusing randomly in a two-well potential. It seems likely, however, that these provocative experiments will not be adequately understood without measurements of the spatial structure to supplement those of the heat flux.

Siggia & Zippelius (1981*a*) have shown that relaxational dynamics based on an amplitude equation has a severely limited domain of validity as the Prandtl number becomes small. One consequence is that convective pattern evolution may resemble the behaviour of a glass in the sense of being transient on a time-scale that diverges exponentially with the system size, so that one may in practice never get to a stable time-independent flow in a sufficiently large cell. Siggia & Zippelius (1981*b*) have also calcuated both analytically and numerically the behaviour of defects consisting of extra rolls extending into an otherwise regular convection pattern. They were found to move at constant velocity parallel to the roll axis.

Manneville (1981) has presented preliminary numerical simulations of pattern evolution in a cylindrical geometry (radius-to-depth ratio of 5·4) based on an amplitude equation. The resulting contour plots seem qualitatively similar in many respects to those presented in figures 4 and 5 of the present paper.

4.3. *Skewed varicose and oscillatory instabilities*

The oscillatory instability, in which transverse waves propagate along the roll axis, was discussed theoretically by Clever & Busse (1974) and was already apparent in the photographs of Willis & Deardorff (1970). Since then, it has been noted in many experiments at low Prandtl number. Busse & Clever (1979) later noted that the skewed varicose instability, in which the rolls develop a periodic thickness modulation along their length, actually occurs at lower R (unless the roll wavenumber is

abnormally low). Using controlled initial conditions, they were able to observe this instability. It seems not to have been previously identified as having an essential role in the onset of noisy time dependence.

McLaughlin & Orszag (1982) have performed a numerical study of convective instabilities by integrating the three-dimensional time-dependent Boussinesq equations at a Prandtl number of 0·71. They observe the oscillatory instability, but the skewed varicose instability is suppressed by the small lateral size of their layer.

There are no previous measurements to our knowledge of the time-averaged roll structure in the noisy regime above the onsets of the oscillatory and skewed varicose instabilities, or of the suppression of the fluctuations by local heat sources.

5. Discussion and conclusions

In a bare outline, we find that a large-aspect-ratio convecting fluid at Prandtl number 2·5 is characterized by three regimes as function of Rayleigh number up to $50R_c$: pattern evolution below a threshold R_1; noisy time dependence due to the skewed varicose instability above R_1; and noisy time dependence due to both the skewed varicose and oscillatory instabilities above a threshold R_2.

5.1. *Regime A: pattern evolution*

Below $R_1 = 5R_c$ complex patterns produced by a large change in R gradually evolve (figures 4, 5) towards simple patterns (such as those of figure 2) with fewer defects in which the rolls align approximately perpendicular to the lateral cell boundaries. Defects in the roll pattern (figures 4, 5) are clearly important in the process of pattern evolution and in determining the relative stability of different states. They seem to be of two types: persistent defects associated with boundary-induced curvature in the roll pattern; and isolated defects in a parallel pattern, which quickly translate out of the field of view, as expected from theoretical work (Siggia & Zippelius 1981*b*).

The pattern-evolution phenomena seem qualitatively consistent with the picture presented by Cross (1982), involving competition between boundary, roll curvature, and defect contributions to a Liapunov functional, even though our experiments are mostly performed sufficiently far above threshold that the amplitude equation does not accurately apply. Most notably, this picture implies that defects will persist only when they facilitate perpendicular boundary alignment, as observed.

Runs lasting 9000 vertical thermal diffusion times or 10 horizontal diffusion times are not always long enough to reach a convincingly steady state, although in some cases (figure 3) stability seems to be attained much sooner. There are at least three possible explanations for this failure to reach a steady state in some runs. First, we might still be in the transient regime in spite of the exceptionally long duration of the experiments. Secondly, it is possible that for some initial conditions there is no stable state accessible to the system. Thirdly, there may be many stable states that are able to interact and undergo transitions in the presence of small environmental fluctuations (or possibly intrinsic thermal noise). The third explanation seems most likely to us, especially for large cells. The fact that dissimilar flows are observed even if one attempts to reproduce the initial conditions suggests the existence of many states of comparable stability. The existence of a critical cell size beyond which noise-induced fluctuations would be observed was suggested by Ahlers & Walden (1980). If such a critical size exists, it will presumably also depend on the symmetry, and may be less for cylindrical cells. The exceedingly long timescale of these

phenomena make it difficult to determine whether this hypothetical critical cell size has been exceeded in the present experiments.

5.2. *Regime B: skewed varicose instability*

Above $R_1 = 5R_c$ Doppler imaging shows that the rolls become narrowed and pinch off at irregular intervals (figure 7). This is exactly the behaviour expected from the skewed varicose instability. Furthermore, the onset is quantitatively consistent with that predicted ($4{\cdot}7R_c$) by Busse & Clever (1979) at our Prandtl number and observed roll wavenumber ($2{\cdot}7/d$, where d is the layer depth). The mean roll wavelength increases substantially above $5R_c$, which is another predicted consequence of this instability. For these reasons, it seems safe to associate regime B with the skewed varicose instability.

We find that this instability leads to noisy time dependence with power spectra centred at zero frequency and falling off asymptotically as the negative fourth power (roughly) of the frequency (figures 9, 10). The characteristic frequency (square root of the second moment) increases linearly above the threshold, but seems to be finite at the threshold (figure 8). These statistical properties are similar to those observed previously by Ahlers & Behringer (1978, 1979) and Behringer *et al.* (1980) for the convective heat flux at moderate aspect ratio (ignoring long-timescale phenomena described in §4.2 that are possibly related to stochastically driven pattern changes). The onset of this time dependence at or below $2R_c$ is consistent with that expected for the skewed varicose instability at the lower Prandtl numbers applicable to their experiments. Therefore it seems probable that their observations can also be interpreted in terms of the skewed varicose instability.

The major remaining problem is to understand why this instability produces noise rather than leading to restabilization at a different wavenumber. The non-uniform background roll structure may be responsible. On the other hand, numerical computations by Siggia & Zippelius (1981 *a*) have shown that the instability can result in noise even when it should only be present transiently. The system becomes lost in a complicated phase space. The same mechanism would also apply at higher R where the instability persists.

5.3. *Regime C: oscillatory instability and beyond*

Above $R_2 = 9R_c$ the rolls exhibit transverse oscillations in addition to motions resulting from the skewed varicose instability. This gives rise to a broad spectral peak at finite frequency (figure 6*f*), whose are grows continuously from zero as R is increased. The onset Rayleigh number, the magnitude of the mean frequency f^* at onset, and the evolution of f^* with R (figure 11) are consistent with theoretical predictions for the oscillatory instability. (The comparison is not as precise as one might like because the predictions must be extrapolated to the Prandtl number of this experiment. However, similar behaviour was well documented earlier by Ahlers & Behringer (1979).) Here we note that the two spectral features associated with the skewed varicose and oscillatory instabilities remain distinguishable even at $50R_c$ (figure 6*j*). Furthermore, we find that, even considerably above the onsets of these instabilities, substantial mean structure persists over 1000 vertical thermal diffusion times (figure 12). Thus the stability theory is still relevant far above its domain of quantitative validity.

Our pinning experiments explored the response of the system to externally imposed horizontal thermal anisotropies. We find that the fluctuations (both types) are

inhibited by a line source of heat (figure 14–16), but the heat source must supply a significant fraction of the convective heat transport per wavelength. The fluctuations may be regarded as extremely robust in view of this observation. This result is consistent with the known fact that the instabilities significantly affect the heat transport.

5.4. *Conclusion*

Using automated Doppler imaging techniques, we have shown that three distinct regimes with widely disparate timescales characterize convective flows (at a Prandtl number of 2·5) up to $50R_c$. We expect that the phenomena we observed will dominate over a range of Prandtl numbers (0·5–3, approximately). Below a threshold R_1 the process of slow evolution from complex to simple patterns seems to be qualitatively explained by the competition between surface, bulk, and defect contributions to a Liapunov functional, as proposed by Cross (1982). However, a quantitative study of the domain of validity of this approach has not yet been accomplished, nor is it clear whether the residual time dependence we sometimes observe is a transient or rather a response to external or intrinsic stochastic noise. The skewed varicose and oscillatory instabilities account for the main features of time-dependent convection in the other two regimes above well-defined thresholds R_1 and R_2, and the special role of the skewed varicose instability in the onset of noise has been established.

Overall, there is a remarkable degree of correspondence between stability theory, numerical experiments, and observations. There is still considerable room for progress in quantitatively probing and modelling high-Rayleigh-number phenomena. Doppler imaging has proven to be a powerful tool at moderate Rayleigh numbers where the time-dependence is slow.

This work was supported by the National Science Foundation. We thank M. Heutmacher for experimental assistance, and P. Hohenberg and E. Siggia for numerous helpful conversations.

REFERENCES

AHLERS, G. & BEHRINGER, R. P. 1978 Evolution of turbulence from the Rayleigh–Bénard instability. *Phys. Rev. Lett.* **40**, 712–716.

AHLERS, G. & BEHRINGER, R. P. 1979 The Rayleigh–Bénard instability and the evolution of turbulence. *Prog. Theor. Phys. Suppl.* **64**, 186–201.

AHLERS, G. & WALDEN, R. W. 1980 Turbulence near onset of convection. *Phys. Rev. Lett.* **44**, 445–448.

BEHRINGER, R. P., AGOSTA, C., JAN, J. S. & SHAUMEYER, J. N. 1980 Time-dependent Rayleigh–Bénard convection and instrumental attenuation. *Phys. Lett.* **80A**, 273–276.

BEHRINGER, R. P., SHAUMEYER, J. N., AGOSTA, C. A. & CLARK, C. A. 1982 Onset of turbulence in moderately large aspect ratios. Submitted to *Phys. Rev.* A.

BERGÉ, P. 1981 Rayleigh–Bénard convection in high Prandtl number fluids. In *Chaos and Order in Nature* (ed. H. Haken). Springer.

BUSSE, F. H. & CLEVER, R. M. 1979 Instabilities of convection rolls in a fluid of moderate Prandtl number. *J. Fluid Mech.* **91**, 319–355.

CHEN, M. M. & WHITEHEAD, J. A. 1968 Evolution of two-dimensional periodic Rayleigh–Bénard convection cells of arbitrary wave-numbers. *J. Fluid Mech.* **31**, 1–15.

CLEVER, R. M. & BUSSE, F. H. 1974 Transition to time-dependent convection. *J. Fluid Mech.* **65**, 625–645.

CROSS, M. C. 1982 Ingredients of a theory of convective textures close to onset. *Phys. Rev.* A **25**, 1065–1076.

CROSS, M. C., DANIELS, P. G., HOHENBERG, P. C. & SIGGIA, E. D. 1980 Effect of distant sidewalls on wave-number selection in Rayleigh–Bénard convection. *Phys. Rev. Lett.* **45**, 898–901.

CROSS, M. C., DANIELS, P. G., HOHENBERG, P. C. & SIGGIA, E. D. 1983 Phase-winding solutions in a finite container above the convective threshold. *J. Fluid Mech.* (in press).

DAVIS, S. H. 1967 Convection in a box: linear theory. *J. Fluid Mech.* **30**, 465.

GOLLUB, J. P. 1982 Recent experiments on the transition to turbulent convection. In *Nonlinear Dynamics and Turbulence* (ed. D. Joseph & G. Iooss). Pitman.

GOLLUB, J. P. & BENSON, S. V. 1980 Many routes to turbulent convection. *J. Fluid Mech.* **100**, 449–470.

GOLLUB, J. P. & MCCARRIAR, A. R. 1982 Spatial Fourier analysis of convection patterns. Submitted to *Phys. Rev.* A.

GOLLUB, J. P. & STEINMAN, J. F. 1981 Doppler imaging of the onset of turbulent convection. *Phys. Rev. Lett.* **47**, 505–508.

GREENSIDE, H. S., AHLERS, G., HOHENBERG, P. C. & WALDEN, R. W. 1982 A simple stochastic model of the onset of turbulence in Rayleigh–Bénard convection. *Bell Labs Preprint.*

KIRCHARTZ, K. R., MÜLLER, U., OERTEL, H. & ZIEREP, J. 1981 Axisymmetric and non-axisymmetric convection in a cylindrical container. *Acta Mechanica* **40**, 181–194.

KRISHNAMURTI, R. 1970 On the transition to turbulent convection. Part 1. The transition from two- to three-dimensional flow. *J. Fluid. Mech.* **42**, 295–307.

KRISHNAMURTI, R. 1973 Some further studies on the transition to turbulent convection. *J. Fluid Mech.* **60**, 285–303.

MCLAUGHLIN, J. B. & ORSZAG, S. A. 1982 Transition from periodic to chaotic thermal convection. *J. Fluid Mech.* **122**, 123–142.

MANNEVILLE, P. 1981 Numerical simulation of 'convection' in cylindrical geometry. *CEN Saclay Preprint.*

NEWELL, A. C. & WHITEHEAD, J. A. 1969 Finite bandwidth, finite amplitude convection. *J. Fluid Mech.* **38**, 279–303.

SEGEL, L. A. 1969 Distant sidewalls cause slow amplitude modulation of cellular convection. *J. Fluid Mech.* **38**, 203–224.

SIGGIA, E. D. & ZIPPELIUS, A. 1981*a* Pattern selection in Rayleigh–Bénard convection near threshold. *Phys. Rev. Lett.* **47**, 835–838.

SIGGIA, E. D. & ZIPPELIUS, A. 1981*b* Dynamics of defects in Rayleigh-Bénard convection. *Phys. Rev.* A **24**, 1036–1049.

STORK, K. & MÜLLER, U. 1972 Convection in boxes: experiments. *J. Fluid Mech.* **54**, 599–611.

WILLIS, G. E. & DEARDORFF, J. W. 1970 The oscillatory motions of Rayleigh convection. *J. Fluid Mech.* **44**, 661–672.

WHITEHEAD, J. A. 1976 The propagation of dislocations in Rayleigh–Bénard rolls and bimodal flow. *J. Fluid Mech.* **75**, 715–720.